The role of branching on the ultrafast dynamics and 2-photon absorption of two pyrimidine push-pull molecules

Alexandros Katsidas,[1]Michaela Fecková,[2,3,4] Filip Bureš,[3,4] Sylvain Achelle,[2] Mihalis Fakis[1,*]

[1] Department of Physics, University of Patras, 26500 Greece

[2] Univ Rennes, CNRS, ISCR (Institut des Sciences Chimiques de Rennes)- UMR 6226, F-35000 Rennes, France

[3] Institute of Organic Chemistry and Technology, Faculty of Chemical Technology, University of Pardubice, Studentská 573, Pardubice, 53210, Czechia

[4] Institute of Technology and Business in České Budějovice, Okružní 517/10, České Budějovice, 37001, Czechia

Abstract

The dynamics and 2-photon absorption (2PA) properties of two pyrimidine chromophores are studied by means of femtosecond time-resolved fluorescence and 2-photon excited fluorescence techniques. The pyrimidine is used as an electron withdrawing group and is substituted at the C2 position with phenylacridan fragment while at positions C4/6 diphenylaministyryl donor moieties are appended to afford the pseudo-dipolar and pseudo-quadrupolar molecules, respectively. The chromophore **2** shows more efficient fluorescence emission while **1** exhibits larger Stokes shifts. Their decay pathways are discussed through an emission from a locally excited (LE) and an intramolecular charge transfer (ICT) state. Ultrafast dynamics in tetrahydrofuran show an ICT population for **1** that is faster than solvation while for **2**, due to its pseudo-quadrupolar nature, ICT is slower and takes place from the solvated LE state. Finally, molecule **2** shows better 2PA properties with cross sections reaching 560 GM at 820 nm.

Introduction

Intramolecular charge transfer (ICT) in push-pull π-conjugated organic chromophores is a fundamental process, controlling the nature and dynamics of the excited states, the photophysical properties and the potential for future applications of these chromophores in diverse and emerging photonic applications.[1-6] It also plays a

crucial role in various biophysical phenomena.[7-10] The population of ICT states takes place in chromophores of dipolar, quadrupolar and octupolar topology and not only depends on the electron donating/withdrawing groups and the π-conjugated core but also on the molecular environment. In solution, the polarity of the solvent affects the energy level of the ICT state rendering its population energetically favorable.[11-16] Emission by an ICT state is characterized by a low-energy, broad and structureless emission spectrum with reduced fluorescence quantum yield (Φ), compared to the narrow and vibronically structured emission stemming from a Franck Condon (FC) state.[17-20] Often, the ICT process leads to the population of a number of states with variable degree of charge-transfer (CT) or to an excited state conformation with a twisted morphology (TICT), resulting to a very broad spectrum with dual peaks.[21-27]

The ICT takes place within the excited state lifetime and especially in the 100 fs to a few ps timescale. It often occurs simultaneously with solvent relaxation, structural re-organization and isomerization leading to rich and complicated photodynamics. Separating the above kinetic phenomena is typically a non-trivial task.[28-30] In dipolar (D-π-A) molecules, ICT is typically expected and is easily manifested by significant positive emission solvatochromism. In quadrupolar and octupolar molecules, ICT is related to the excited state symmetry breaking (SB), a phenomenon that has attracted great scientific interest.[31-37] SB is decisively dependent on solute-solvent interactions since the solvent's strong reaction field enhances SB and an excited state of quadrupolar nature relaxes to a dipolar state.

Molecules with ICT properties have been the subject of intense scientific interest since a deep understanding of the control and modulation of ICT is imperative towards an advance in photonic devices. They have demonstrated enhanced electro-optic coefficients,[38,39] second harmonic generation efficiency[40,41] and 2-photon absorption (2PA) properties.[17,42-50] Especially, due to their non-linear optical (NLO) properties, they are attractive for a variety of applications in imaging,[51] photodynamic therapy,[52] optical limiting,[53,54] direct laser microfabrication and 3D optical data storage.[55-57] Moreover, they have also exhibited reverse intersystem crossing (RISC) and excellent thermally activated delayed fluorescence (TADF) properties due to a small singlet and triplet excited state gap.[58-61] Finally, aggregation induced emission (AIE) has also been reported for push-pull structures,[62,63] rendering these ICT molecules highly suitable for next-generation organic light emitting diodes (OLEDs), while they are also finding use in organic solar cells as electron acceptors.[64,65]

As it is easily understood, push-pull molecules with ICT properties are appealing not only from a fundamental point of view but also because of a plethora of applications. Alkyl-amino, phenyl-amino, 9*H*-carbazol-9-yl and acridan fragments are some of the most well-known groups to be used as electron donors.[66-71] On the other hand, various heterocyclic rings have been investigated as electron withdrawing groups in ICT molecules such as benzothiazole and triazine.[72-75] The pyrimidine group with two nitrogen atoms has been used as a suitable fragment in NLO chromophores, in TADF emitters as well as in stimuli responsive fluorescence switches.[76-79] In a recent work of ours, we have reported on the synthesis of six 4-styryl or 4,6-distyryl substituted pyrimidines linked to acridan at the C2 position via a phenylene linker. We have focused on their dual emission properties and long-lived ICT states.[80]

As a continuation of our previous work, we focus herein on the ultrafast dynamics and NLO properties of two of the previously reported pyrimidines, having diphenylamino donors connected to the styryl fragments. Ultrafast dynamics reveal emission by a locally excited (LE) and ICT state which are both solvent relaxed while good 2PA values are found. Based on ultrafast dynamics and 2PA measurements, it is concluded that the acridan group does not play a role in the emission process as it lies almost perpendicular to the adjacent phenyl ring.

Experimental

Steady state spectroscopy

The two molecules were examined for their steady state spectra in hexane (HEX), decane (DEC), toluene (TOL), tetrahydrofuran (THF), dichloromethane (DCM), acetone (ACT) and acetonitrile (MeCN). The absorption spectra were detected with a Schimadzu UV-3000 spectrometer while a Horiba S2 Jobin Yvon Fluoromax 4 was used for the steady-state fluorescence spectra. The Φ values were determined relative to that of 9,10-bis(phenylethynyl)anthracene in cyclehexane (Φ= 1.00).[80]

The time resolved fluorescence dynamics were studied in the ps-ns and fs-ps timescale by means of the Time Correlated Single Photon Counting (TCSPC) and the femtosecond upconversionmethods.[32,81] In the former, a ps diode laser at 400 nm, with 60 ps pulse duration was used as the excitation source. The detection was made under magic angle conditions for the determination of the lifetimes, while anisotropy measurements were also made to determine the rotational time. The overall temporal resolution of the technique was 80 ps. For the

upconversion measurements, a fs mode-locked Ti:Sapphire laser with 80 fs pulses was used. The second harmonic beam at 400 nm played the role of the excitation beam. The temporal resolution of the system was 250 fs. Again, both magic angle and anisotropy measurements were made. For the latter, the polarization plane of the excitation laser was changed by means of a Berek compensator. In both techniques the time resolved anisotropy was calculated by means of $r(t) = \frac{I_{par}(t) - I_{per}(t)}{I_{par}(t) + 2I_{per}(t)}$ where $I_{par}(t)$ and $I_{per}(t)$ are the fluorescence intensities with parallel and perpendicular polarizations to the excitation source's polarization plane. For the TCSPC a correction factor G was determined to compensate for the different response of the monochromator at the two perpendicular polarizations. For the upconversion technique, this factor is unity.

All the samples were fluorescent chromophores, so their 2PA properties were examined by a 2-photon excited fluorescence (2PEF) technique from 730 to 870 nm, using the same mode-locked Ti:Sapphire fs laser described above.[82-84] The 2PA fluorescence intensity was detected as a function of the excitation power, which was changed by a half-wave plate and a polarizer, always validating the square-law dependence. For these measurements, the 2PA cross sections (δ_{2PA}) were calculated using Rhodamine 6G in MeOH (2×10^{-5}M) as the reference sample. The measured scattered light from the solvent has been subtracted.

Materials

Figure 1 shows the chemical structures of the two herein studied push-pull molecules **1** and **2** bearing pyrimidine-based electron acceptor central core. The pyrimidine is substituted at position C2 with phenylacridan group. Also, diphenylamino substituted styryl moieties are appended in the positions C4/6. The synthesis, using cross-coupling and Knoevenagel reactions, has been described previously, together with thermal properties, X-ray analysis and DFT-calculated parameters.[85] It was revealed that the acridan moiety has a perpendicular arrangement with respect to the residual π-system. Besides, non-zero ground state dipole moment was found while the compounds possess no symmetry.

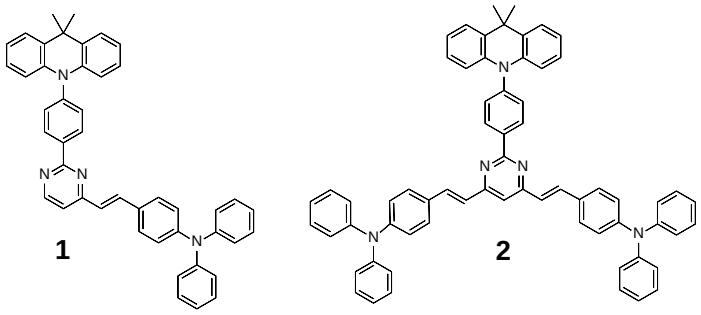

Figure 1. The chemical structures of the pyrimidine-based molecules **1** and **2**.

Steady state spectroscopy

The fundamental optical properties of chromophores **1**and **2** were recorded in solutions with solvents of different polarity. Figure 2 shows the absorption and emission spectra of the two molecules. Table 1 summarizes the photophysical results. The absorption spectra show a main peak at 400-430 nm attributed to the HOMO-1 to LUMO transition.[85] In the apolar solvents HEX and DEC, both molecules feature narrower absorption spectra together with an absorption shoulder due to vibronic coupling. As the polarity is increased, the spectra lose their structure and become broadened, pointing to a ground state with a small degree of ICT nature. Indeed, the ground state dipole moment was found by DFT calculations equal to 6.5 and 5.3 D.[85] The smaller value for **2** is due to its weaker degree of ICT character because of its pseudo-quadrupolar nature. The absorption maximum experienced a hypsochromic shift when the solvent changes from the medium polarity solvent TOL to more polar ones like MeCN.[18]An exception is evident however in DCM. For **2**, the absorption spectra are red-shifted compared to **1** (by about 0.216 eV) which is typical for molecules with longer conjugation length, indicating an electronic coupling between the branches at position C4 and C6. Such an electronic coupling is typical for branched compounds with a nitrogen atom as a central core while it is hindered in the case of a benzene core because of a suppression of coherent interactions among the branches.[86-88]

As a quantitative investigation, the absorption transition dipole moments for **1** and **2** were calculated through the equation[89]

$$\mu_{GE}=9.854\times10^{-2}\left[\frac{1}{n}\frac{1}{[f(n)]^2}\int_{S1}\frac{\epsilon(\nu)}{\nu}d\nu\right]^{1/2}$$

where n is the refractive index of the solvent, $f(n)$=3n/(2n^2+1) and ϵ (ν) is the molar absorption coefficient. The results of these calculations are presented in Table S1. μ_{GE}, in the various solvents, ranges from 5.93 to 7.60 D for **1** and from 10.29 to 11.03 D for **2**, following the differences in the molar absorption coefficient. For **2**, μ_{GE} is higher than **1**, as expected for a molecule with increased conjugation length.

The emission spectra are more sensitive to solvent polarity as shown in Figure 2. In apolar solvents, both molecules feature structured and narrow spectra with clear vibronic peaks. The mirror image rule is far from being obeyed in apolar solvents and this is due to an emission originated from a planar rigid structure because of an increase in the torsional barrier in the excited state.[90,91] On the other hand, in the ground state, the barrier is decreased leading to an absorption from a variety of torsional arrangements. As the polarity increases, the spectra become broader, structureless and the peak is shifted to longer wavelengths, revealing the population of an ICT state which becomes the emitting state in polar environments. Finally, the fluorescence Φ values were measured for four representative solvents and were found significantly higher for **2** *vs.* **1** reaching 0.94 in DCM.

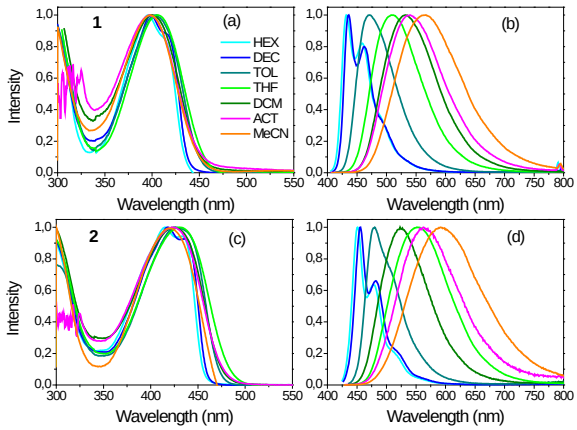

Figure 2. Absorption (a, c) and emission (b, d) spectra of molecules **1** and **2** in various solvents.

Table 1: Optical properties of molecules **1** and **2**.

Molecule	Solvent	λ_{abs}(nm) / ϵ ($mM^{-1}cm^{-1}$)	λ_{em}(nm)	Φ	Stokes Shift (cm^{-1})	τ(ns)[a]	δ_{2PA}(GM)
1	HEX	396 / 24.4	432, 459	0.23	2100	0.87	150
	DEC	399	436, 463	-	2130	1.07	
	TOL	404 / 26.1	471	0.35	3520	1.44	110

	THF	400 / 34.0	508	0.47	5310	2.42	130
	DCM	406 / 31.3	532	0.75	5830	2.80	
	ACT	397	540	-	6670	2.96	
	MeCN	398	566	-	7460	2.91	
2	HEX	415, 433 / 65.1	451, 479	0.52	1920	1.25	560
	DEC	417, 436	456, 482	-	2050	1.36	
	TOL	426 / 62.1	480	0.65	2640	1.53	460
	THF	424 / 65.6	523	0.61	4460	2.38	460
	DCM	430 / 58.0	553	0.94	5170	2.89	
	ACT	422	563	-	5930	2.49	
	MeCN	419	592	-	6970	1.84	

[a] Taken as the average of the lifetimes measured by the TCSPC technique.

To obtain a clearer view on the effect of polarity on the steady state spectra, the Lippert-Mataga plots were constructed *i.e* the Stokes shift was plotted as a function of solvent polarizability (Figure S1). As can be seen, molecule **2** has a slightly smaller Stokes shift for all the solvents and also a slightly smaller slope of the Lippert-Mataga plot. From the slope of these plots, the change of the permanent dipole moments $\Delta\mu_{solv}$ upon excitation can be calculated following the equation:[18,92,93]

$$v_A - v_F = \frac{2(\mu_E - \mu_G)^2}{hca^3}\Delta f + constant$$

Where h is the Planck's constant, a is the Onsager cavity radius and $\mu_E - \mu_G$ is the change of the dipole moments $\Delta\mu_{solv}$. The solvent's polarizability is given by the equation:

$$\Delta f = f(\varepsilon) - f(n^2) = \frac{\varepsilon - 1}{2\varepsilon + 1} - \frac{n^2 - 1}{2n^2 + 1}$$

where ε is the dielectric constant and n is the refractive index of the solvent. Table S2 summarizes these values for all solvents. For pseudo-dipolar chromophore **1**, the Onsager radius was estimated from its DFT-optimized structure as half of the distance between the Ph_2N donor occupied by the HOMO–1 and the LUMO spread over the central pyrimidine acceptor. For pseudo-quadrupolar **2**, the longest distance for the charge separation corresponds to the Ph_2N-centered HOMO–1 and the opposite olefinic linker bearing the LUMO (Figure S13).[X] Finally, $\Delta\mu_{solv}$ was found 9.85 D for **1** and 17.47 D for **2** respectively (Table S3).

Excited state dynamics

Fluorescence dynamics in the nanosecond timescale

To further investigate the mechanisms that occur after excitation, we performed TCSPC measurements, thus determining the excited states' lifetimes. The experimental results and fitting parameters are shown in Figure 2 and Table S4 respectively. For both molecules the fluorescence lifetime is in the range of ns and increases as the polarity is increased from the apolar HEX to medium polar DCM, owing to the stabilization of the ICT state, e.g. for **2**, the lifetime is 1.25 ns in HEX and 3.27 ns in DCM. In the most polar solvents ACT and MeCN, the lifetime decreases compared to the medium polarity ones, revealing that as the ICT state is shifted to lower energies, nonradiative pathways become significant. However, this lifetime decrease is not very important, compared to other push-pull molecules where a more than one order of magnitude decrease is observed.[34,81] The decay curves of molecule **2** are fitted with a single-exponential function in low polarity solvents while a two-exponential one is needed as the polarity increases. Based on these findings and the steady state spectra, $\tau_1$can be attributed to the lifetime of the LE state while τ_2 to the ICT state. For **1**, the discussion on the lifetimes is similar excluding the two apolar solvents HEX and DEC where a short lifetime of ~ 0.70 ns exists, whose amplitude however reduces significantly in the latter solvent. This can be tentatively attributed to an unrelaxed excited state which then relaxes to form a LE state with lifetime of 1.0-1.87 ns. Using the Φ values for HEX, TOL, THF and DCM and the average lifetimes, the radiative (k_{rad}) and non-radiative (k_{nrad}) decay rates were calculated (Table S5). $k_{rad}$was in all cases higher for **2** ranging from 0.26 to 0.42·10^9 s^{-1}.

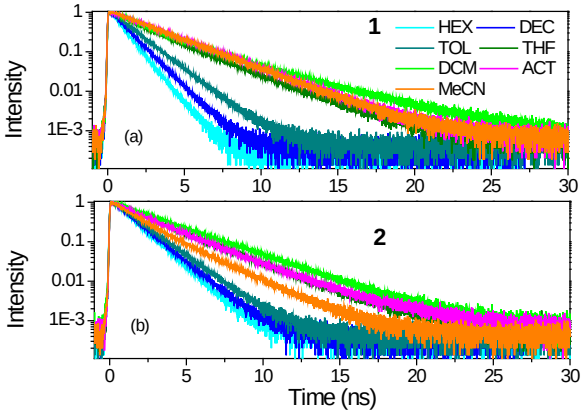

Figure 2. Fluorescence decays in the nanosecond timescale for **1** and **2** in various solvents. Exc.: 400 nm, detection at the peaks of the emission spectra.

Next, the emission transition dipole moment is calculated using the lifetimes obtained by the TCSPC method and the following equation[89]

$$\mu_{EG}=1785.7\left[\frac{\Phi}{\tau n^3}\frac{1}{[f(n)]^2}\frac{1}{\tilde{\nu}_f^3}\right]^{1/2}$$

Φ is the fluorescence quantum yield, τ the average excited state lifetime, n the solvent refractive index, $f(n)=3n/(2n^2+1)$ and $\tilde{\nu}_f^3$ is the average cubic fluorescence frequency expressed by:

$$\tilde{\nu}_f^3=\frac{\int I(\nu)\,\mathrm{d}\nu}{\int I(\nu)/\nu^3\mathrm{d}\nu}$$

μ_{EG} can also provide useful information for the nature of the excited state. The values are summarized in Table S1 and are higher for 2 (e.g. μ_{EG} for **2** in DCM is 9.53 vs 8.26 D for **1**) following the changes of the quantum yields.

Fluorescence dynamics in the femtosecond-picosecond timescale

The above-described fluorescence dynamics in the nanosecond timescale provided information on the decay pathways of the molecules. To gain a deeper insight into the time evolution of the systems' excited states, fluorescence up-conversion measurements were carried out and the dynamics were examined within the first 130 ps in TOL and THF solutions. Because of the wavelength dependent nature of the dynamics in this short timescale, various measurements at different emission wavelengths were detected.

The dynamics along with the time-resolved emission spectra (TRES) and time-resolved area normalized emission spectra (TRANES) for TOL and THF are shown in Figures 3 and 4 for **1** and **2** respectively.[94-98] The 2D plots of the TRES are shown in figure S2. In all samples, a fast decay is observed at the shorter wavelengths and a slow rise at the longer ones. This effect is due to a relaxation of the excited state towards lower energies originated by solvent relaxation and ICT population and leads to a red-shift of the emission spectrum. The curves were analyzed using a global fit method and the fitting results for the two faster mechanisms are shown in tables S6 and S7. In all cases, a three-exponential fitting was needed to fit the results. The third component was fixed to be equal to the lifetime found by the TCSPC technique. Within the ps timescale, two decay lifetimes of the order of ~1.3 ps and 5.9-6.6 ps in TOL and 0.6-0.8 and 2.5-2.8 ps in THF were found. The lifetimes correspond to decay mechanisms at short wavelengths (positive amplitudes) while they evolve to rise

mechanisms (negative amplitudes) at longer ones. The relaxation times are smaller in THF for both molecules, because it is a more polar solvent than TOL and the solute-solvent interactions are stronger. In both solvents, the relaxation times are similar to solvation times for TOL and THF but as will be shown below, ICT population is also taking place apart from solvation.[99,100]

The TRES of **1** in TOL exhibit a small transient red-shift (374 cm^{-1}) which is finished within ~ 10 ps, while the TRES of **2** remain almost unchanged with only a slight broadening. On the other hand, in THF the spectral changes are more obvious with the spectra of both molecules having a significant redshift (1313 cm^{-1} and 1171 cm^{-1} for **1** and **2** respectively) within 10 ps. The solvent response function $C(t)$ for both molecules and solvents is plotted in Figure S3. $C(t)$ decays faster in THF pointing to a more efficient spectral relaxation. A bi-exponential function was used to fit $C(t)$ with lifetimes similar to those found after global analysis of the individual dynamics pointing to inertial and diffusive solvation mechanisms (Table S8). The total area-normalized intensity obtained by the TRES is also plotted in Figure S3 and its dynamics is visually compared to the $C(t)$. In toluene, the total intensity exhibits a rise up to 2 ps, possibly due to vibronic relaxation. It is obvious that spectral relaxation is faster in toluene, while in the more polar THF, the spectral relaxation is highly related to the quenching of the excited state. Apart from the transient red-shift, the spectra are also accompanied by a gradual broadening indicating a decay process involving more than one emitting state.[17,29] Figure S4 shows the FWHM of the TRES as a function of time. Especially in the case of THF, for both compounds, an initial decrease of the FWHM is observed. This is due to a fast decay of the high energy rotamers to a rigid excited state.

Finally, following the method described by Vauthey et al.[101] and used by Xia et al.[102] the instantaneous emission dipole moment $\mu_{EG}(t)$, is calculated at different times for **1** and **2** in THF. The time dependence of $\mu_{EG}(t)$ is shown in Figure S5 in non-normalized and normalized units. For both molecules, $\mu_{EG}(t)$ decreases within the first 10 ps reaching a constant value at longer times which is equal to the emission dipole moment of the relaxed excited state as calculated by eq. 2. The decrease of $\mu_{EG}(t)$ is associated to a change in the nature of the excited state. The initial values of $\mu_{EG}(t)$ found 9.5 and 7.5 D for **1** and **2** respectively are considered as the emission dipole moments of the LE state. The more intense decay of $\mu_{EG}(t)$ for 2 points to a change of its excited state from LE with a pseudoquadrupolar nature to an excited state with a CT character.

Although the TRES provide a quantitative aspect of the spectral changes, a further insight on the photodynamic mechanisms is obtained by observing the TRANES (Figures 3 and 4). In TOL, both molecules have an isoemissive point indicating that there are two emissive species. The transient spectral changes for **1**, as mentioned above, are stronger than those of **2** which could be ascribed to its dipolar nature, also revealed by the time resolved anisotropy and 2PA measurements (vide infra). The two emissive species could be considered as the LE and ICT state, while the contribution of the latter is less significant in the case of **2**. On the other hand, the two molecules reveal different and more pronounced behavior in THF. **1** exhibits an isoemissive point within the first 2 ps, while a gradual redshift of the spectrum takes place at longer times and the isoemissive point is lost (Figure S6). The isoemissive point at short timescales, is due to an emission from the LE and ICT states with peaks at 21000 cm^{-1} and 20220 cm^{-1}, the latter being populated on a ~ 100 fs time scale i.e within the inertial solvation time for THF. Then, the emission from the ICT state dominates and it relaxes at longer times (2-10 ps) leading to the observed transient red-shift to 19700 cm^{-1}. Molecule **2** in THF shows exactly the opposite behavior. Initially, the spectrum experiences a transient shift in <3ps (without an isosbestic point) due to an inertial and diffusion relaxation of the LE state by the solvent molecules from 20300 cm^{-1} to 19500 cm^{-1} (Figure S7). After 3 ps, an isoemissive point is revealed which is an indication of the population of an ICT state (at 19100 cm^{-1}) by energy transfer from the relaxed LE state and the simultaneous emission of both states. Figure S8 shows an energy diagram that is used as a model for the explanation of the dynamics for **1** and **2** in THF. The population of the ICT state for **2** is slower than for **1**, taking place after solvation, while the ICT population for **1** is within the inertial solvent relaxation. This is attributed to the quadrupolar nature of **2** compared to the dipolar character of **1**.

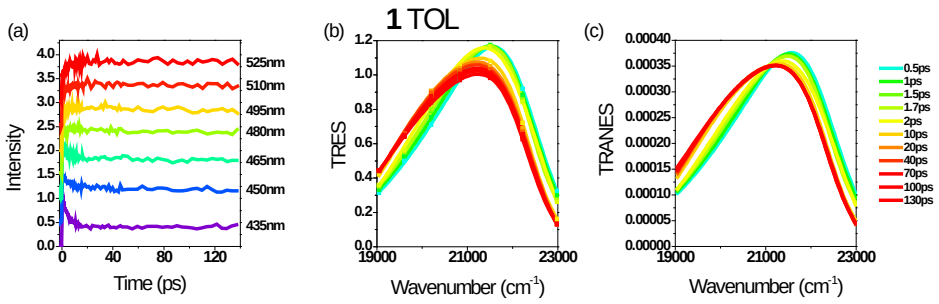

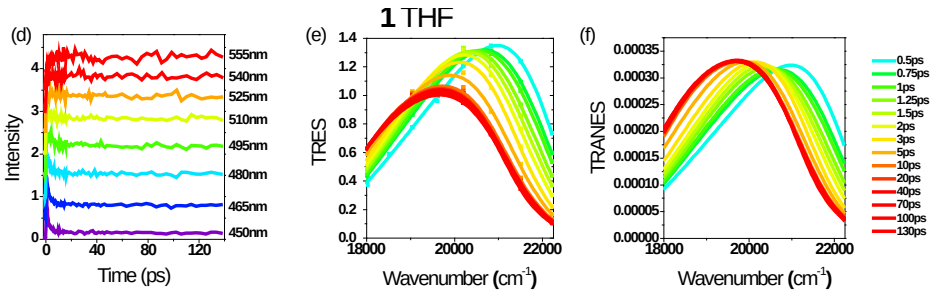

Figure 3. (a), (d) Fluorescence dynamics at selected wavelengths, (b), (e) TRES and (c), (f) TRANES for **1** in TOL and THF.

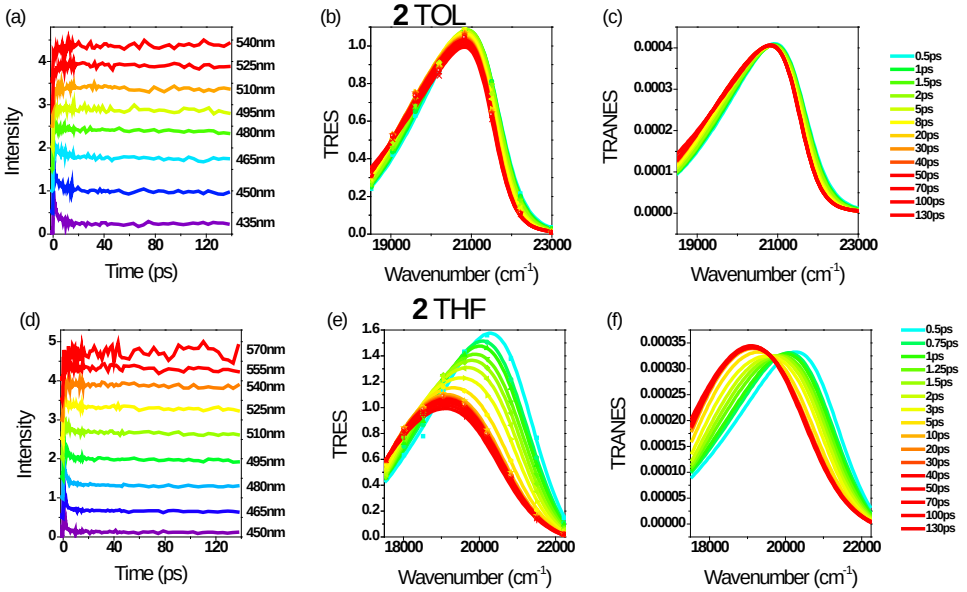

Figure 4. (a), (d) Fluorescence dynamics at selected wavelengths, (b), (e) TRES and (c), (f) TRANES for **2** in TOL and THF.

Anisotropy dynamics

In our previous work, DFT analysis in molecules **1** and **2** revealed that the acridan moiety is rotated and lies off plane with respect to the pyrimidine core, therefore, it is not expected to play a crucial role in the optical properties and ICT process. To confirm this assumption, anisotropy measurements in the fs-ps time scale were conducted and the plots are shown in Fig. 5.

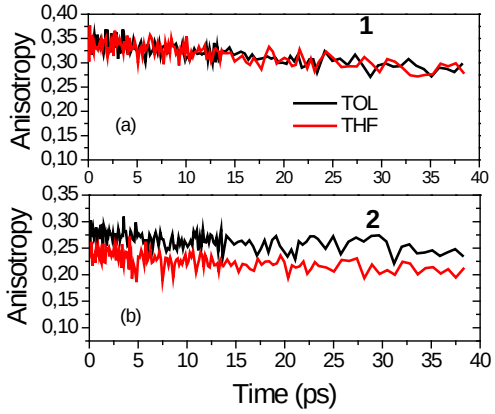

Figure 5. Anisotropy dynamics within the first 40 ps measured by the up-conversion technique, for **1** (a) and **2** (b) in TOL and THF

The initial anisotropy r_0 provides an aspect of the molecular symmetry after excitation. For dipolar molecules, r_0 is expected to be close to 0.4 while for quadrupolar and octupolar ones it is expected to be close to 0.2 and 0.1 respectively. For **1** and **2**, r_0 is 0.35 and 0.24-0.27, i.e close to the values expected for a dipolar (D-π-A) and quadrupolar (D-π-A-π-D) symmetry. Also, no decay of the anisotropy in the 100s fs to ps timescale was observed for **2**, as expected for octupolar molecules due to coherent and incoherent energy delocalization mechanisms among the branches. Anisotropy decays in the ns timescale were also performed to determine the rotational correlation time τ_{cor} as a function of solvent viscosity. τ_{cor} ranges from 0.15 ns to 0.38 ns for **1** and from 0.25 to 0.67 for **2** and is linearly dependent on the solvent viscosity (Figures S9, S10 and Table S9).

2-photon Absorption properties

The 2PA spectra are presented in Figure 6 for both molecules in HEX, TOL and THF. The 2-photon induced fluorescence as a function of excitation intensity is shown in Figure S11 exhibiting the quadratic dependence as expected for a 2PA process. As expected, **2**, due to its longer conjugation length, has larger 2PA cross sections than its dipolar counterpart reaching 560 GM in HEX and 450 GM in TOL and THF. Apart from the difference in the 2PA values, the 2PA peak of **2** falls within the same spectral region as that of **1** meaning that the spectral shift observed in their 1PA spectra is not maintained. This is due to a difference in molecular symmetry. 2PA spectroscopy is, in general, useful in identifying the nature and molecular geometry of the excited states.[103] A comparison of 2PA spectra with the rescaled 1PA ones is shown in Figure S12. For **2**, the 2PA peak is blue-

shifted compared to twice the wavelength of the rescaled 1PA peak, following the expected behavior of a quadrupolar molecule based on the Frenkel exciton model.[33,87,104] Besides, the 2PA and rescaled 1PA spectra of **1** coincide, providing further evidence for its pseudo-dipolar behavior as also concluded by the fs-anisotropy measurements.

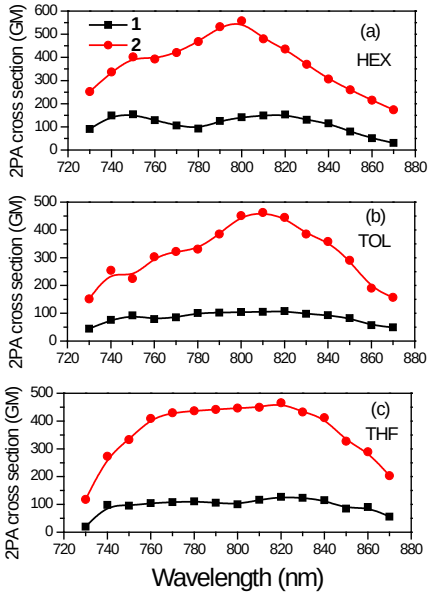

Figure 6. 2PA spectra of **1** and **2** in (a) HEX, (b) TOL and (c) THF.

Mono and di(diphenylamino)styrylpyrimidines have been extensively studied in the past for their 2PA properties.[76] In this frame, the effect of electron donating group, the effect of branching and π-conjugated bridge has been addressed.[105-107] Surprisingly, very large 2PA cross section values have been found reaching 3000 GM. However, great care must be taken in discussing and comparing different results since in certain cases very high excitation powers and sample concentrations have been used. On the other hand, a comparison of the 2PA values of **1** and **2** can be made with those of the molecules presented in a previous work of ours[50] where the acridan group is replaced by another diphenylamino substituent, addressing the influence of the C2 substitution. Interestingly, the three-branched A-(π-D)$_3$ compound with diphenylamino groups at the periphery (2c in ref. 50) has very similar 2PA cross section values and peak wavelengths compared to **2**, showing that the

replacement of the diphenylamino with the out of plane acridan does not play a decisive role in the 2PA properties.

Finally, the 2PA results are also useful in calculating again the difference between the excited and ground state dipole moments using the equation:[108,9]

$$\Delta\mu_{2PA} = \left(\frac{5}{4(1+2cos^2\theta)} \frac{hcN_A}{\pi 10^3 ln10} \frac{n}{f_{opt}^2} \frac{\nu_{max}}{\varepsilon_{max}} \delta_{2PA}(0-0) \right)^{1/2}$$

where ν_{max} is the lowest energy absorption frequency (in Hz), ε_{max} is the peak molar absorption coefficient (in mol^{-1} dm^3 cm^{-1}), θ is the angle between the dipole moments of the excited and ground states (considered as θ = 0), n is the refractive index and f_{opt} is the local field factor equal to $(2 + n^2)/3$.The difference in the permanent dipole moments of the ground and excited states was calculated and compared with those found from the solvation method. $\Delta\mu_{2PA}$ in TOL was found 12.9 and 17.00 D for **1** and **2** respectively being in reasonable agreement with those found by means of the Lippert-Mataga plots (Table S3).

Conclusions

In summary, we have investigated the role of branching on the steady-state, excited state dynamics and 2PA properties of two pyrimidine molecules with phenylacridan group at the C2 position. The pyrimidine was also substituted at the C4/6 positions(s) with styryl groups attached to diphenylamino donors to obtain molecules **1** and **2**. Steady state spectroscopy shows larger Stokes shift for molecule **1**, while higher fluorescence quantum yields were found for **2**. The time-resolved fluorescence measurements revealed emission pathways attributed to emission by an LE and ICT states. For **1** in THF, the ICT population takes place as fast as inertial solvation, followed by diffusive solvation of the ICT state. On the other hand, for **2**, LE to ICT energy transfer is slower than for **1**, occurring by the solvated LE state. Time resolved anisotropy measurements in the fs-ps timescale showed an excited state of dipolar and pseudoquadrupolar nature for **1** and **2** respectively. Finally, 2PA characterization showed a more than 4-times increase of the 2PA cross sections for **2** *vs.* **1**, reaching 560 GM at 820 nm in HEX.

Acknowledgements

Part of this work was supported from ERDF ‘‘Innovative materials suitable for high added value applications (INMA)’’ (No. CZ.02.01.01/00/23_021/0008593). M. F. acknowledges the Région Bretagne, France, for her Ph. D. funding (HOLED project).

Supporting Information

The role of branching on the ultrafast dynamics and 2-photon absorption of two pyrimidine push-pull molecules

Alexandros Katsidas,[1]Michaela Fecková,[2,3,4] Filip Bureš,[3,4] Sylvain Achelle,[2] Mihalis Fakis[1,*]

[1] Department of Physics, University of Patras, 26500 Greece

[2] Univ Rennes, CNRS, ISCR (Institut des Sciences Chimiques de Rennes)- UMR 6226, F-35000 Rennes, France

[3] Institute of Organic Chemistry and Technology, Faculty of Chemical Technology, University of Pardubice, Studentská 573, Pardubice, 53210, Czechia

[4] Institute of Technology and Business in České Budějovice, Okružní 517/10, České Budějovice, 37001, Czechia

Table S1. Transition dipole moments for **1** and **2** in HEX, TOL, THF and DCM.

Molecule	Solvent	μ_{GE} (D)	μ_{EG} (D)	Φ
1	HEX	5.93	6.54	0.23
	TOL	6.50	6.41	0.35
	THF	7.57	6.68	0.47
	DCM	7.60	8.26	0.75
2	HEX	10.29	8.54	0.52
	TOL	10.42	8.76	0.65
	THF	11.03	8.00	0.61
	DCM	10.62	9.53	0.94

Table S2. Solvent parameters. ε: dielectric constant, n: refractive index, $f(\varepsilon)$ and $f(n^2)$ the low and high-frequency polarizabilities respectively.

Solvent	ε	n	$f(\varepsilon)$	$f(n^2)$
HEX	1.88	1.37	0.185	0.186
DEC	2	1.41	0.200	0.199
TOL	2.38	1.49	0.239	0.227

THF	7.58	1.41	0.407	0.197
DCM	8.93	1.42	0.420	0.203
ACT	20.7	1.36	0.464	0.180
MeCN	37.5	1.34	0.480	0.175

Table S3. Onsager radius estimated from the DFT-optimized structures of **1** and **2** (see Figure S13) and the difference in the dipole moments of the ground and excited stare measured by the solvation $\Delta\mu_{solv}$ and 2PA $\Delta\mu_{2PA}$ methods.

Molecule	Onsager radius (Å)	$\Delta\mu_{solv}$ (D)	$\Delta\mu_{2PA}$* (D)
1	4.00	9.85	12.96
2	6.00	17.47	17.00

- $\Delta\mu_{2PA}$ was determined using the 2PA data in TOL.

Table S4. Fitting parameters of the TCSPC fluorescence decays for **1** and **2** in different solvents.

Molecule	Solvent	A1	τ1(ns)	A2	τ2(ns)	A3	τ3(ns)	<τ>(ns)
1	HEX	0.54	0.76	0.46	1.01	-	-	0.87
	DEC	0.15	0.72	0.85	1.13	-	-	1.07
	TOL	-	-	1	1.44	-	-	1.44
	THF	-	-	0.42	1.65	0.58	2.99	2.42
	DCM	-	-	0.60	1.87	0.40	4.19	2.80
	ACT	-	-	-	-	1	2.96	2.96
	MeCN	-	-	-	-	1	2.92	2.91
2	HEX	-	-	1	1.25	-	-	1.25
	DEC	-	-	1	1.36	-	-	1.36
	TOL	-	-	1	1.53	-	-	1.53
	THF	-	-	0.20	0.57	0.80	2.82	2.38
	DCM	-	-	0.15	0.73	0.85	3.27	2.89
	ACT	-	-	0.46	1.69	0.54	3.19	2.49
	MeCN	-	-	0.46	1.15	0.54	2.42	1.84

Table S5. Radiative k_{rad} and non-radiative k_{nrad} rates for **1** and **2** in HEX, TOL, THF and DCM.

Molecule	Solvent	Φ	τ (ns)	k_{rad} (10^9 s^{-1})	k_{nrad}(10^9 s^{-1})
1	HEX	0.23	0.87	0.26	0.88
	TOL	0.35	1.43	0.24	0.45
	THF	0.47	2.42	0.19	0.22
	DCM	0.75	2.8	0.27	0.089
2	HEX	0.52	1.25	0.42	0.38
	TOL	0.65	1.53	0.42	0.23
	THF	0.61	2.38	0.26	0.16

	DCM	0.94	2.89	0.32	0.021

Table S6. Fitting parameters of the upconversion dynamics for **1** and **2** in TOL.

Sample	Wavelength (nm)	A1	τ1 (ps)	A2	τ2 (ps)
1	435	0.15	1.33	0.52	5.94
	450	0.083		0.20	
	465	-0.040		0.13	
	480	-0.130		0.02	
	495	-0.159		-0.10	
	510	-0.10		-0.16	
	525	-0.125		-0.18	
2	435	0.55	1.23	0.31	6.64
	450	0.18		0.33	
	465	-0.03		0.22	
	480	-0.03		0.01	
	495	-0.09		0.03	
	510	-0.097		-0.11	
	525	-0.07		-0.17	
	540	-0.10		-0.13	
	435	0.55		0.31	

Table S7. Fitting parameters of the upconversion dynamics for **1** and **2** in THF.

Sample	Wavelength (nm)	A1	τ1 (ps)	A2	τ2 (ps)
1	450	0.86	0.81	0.29	2.81
	465	0.37		0.51	
	480	-0.14		0.62	
	495	-0.47		0.47	
	510	-0.54		0.30	
	525	-0.52		0.04	
	540	0.06		-0.19	
	555	-0.19		-0.29	
	450	0.99		0.24	
	465	0.65		0.41	
	480	0.30		0.54	

2	495	0.059	0.61	0.52	2.54
	510	-0.12		0.38	
	525	-0.40		0.26	
	540	-0.56		-0.01	
	555	-0.51		-0.09	
	570	0.20		-0.29	

Table S8. Fitting parameters of the solvent response function $C(t)$for **1** and **2** in TOL and THF.

Molecule	Solvent	τ1 (ps)	τ2 (ps)
1	TOL	1.14	5.39
	THF	0.42	3.51
2	TOL	1.44	4.42
	THF	0.37	2.54

Table S9. Initial anisotropy (r_0) and correlation time (τ_{cor}) for **1** and **2** in solvents of various viscosities.

Molecule	Solvent	Viscosity (cP)	r_0	τ_{cor}(ns)
1	HEX	0.33	0.33	0.15
	DEC	0.92	0.32	0.38
	TOL	0.59	0.37	0.27
	THF	0.55	0.31	0.23
	DCM	0.44	0.34	0.19
	ACT	0.32	0.38	0.17
	MeCN	0.37	0.39	0.18
2	HEX	0.33	0.28	0.25
	DEC	0.92	0.24	0.67
	TOL	0.59	0.19	0.46
	THF	0.55	0.22	0.41
	DCM	0.44	0.23	0.37
	ACT	0.32	0.24	0.26
	MeCN	0.37	0.27	0.30

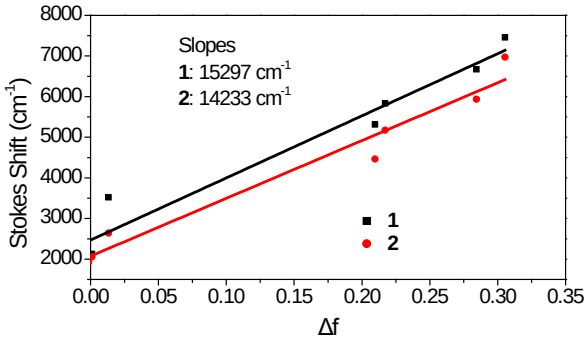

Figure S1. Lippert-Mataga plots for **1** and **2**.

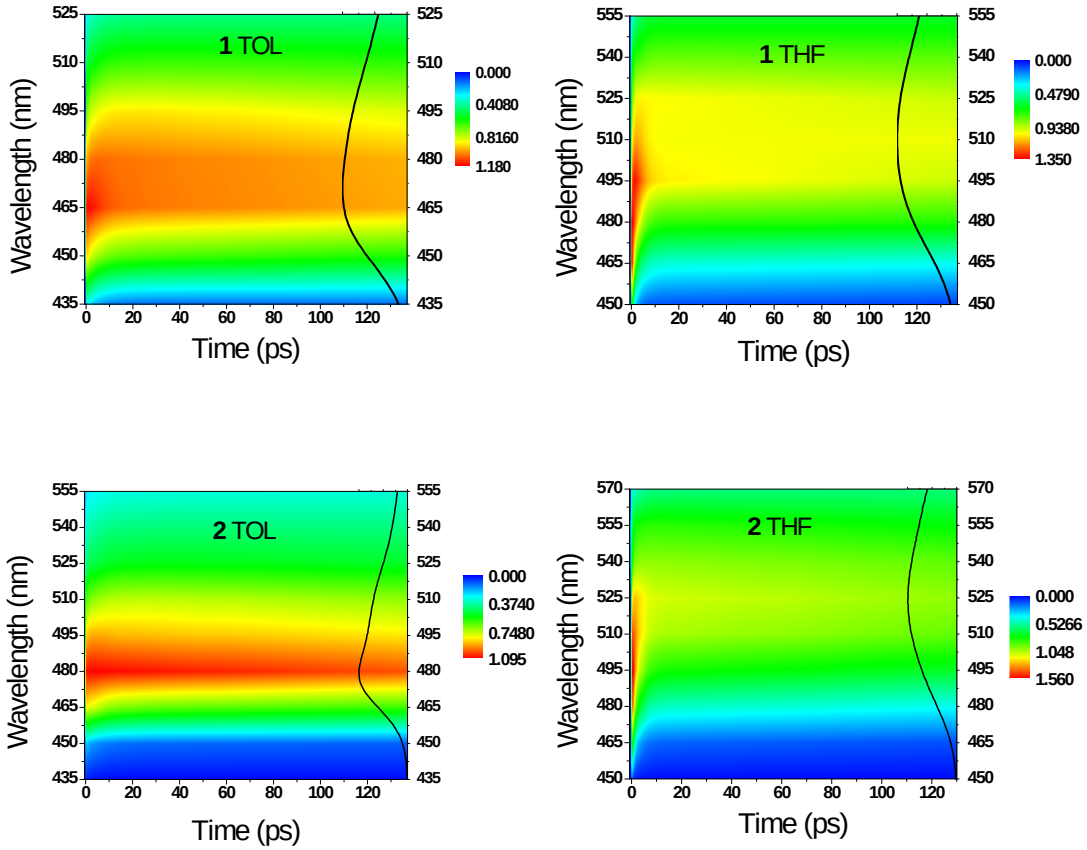

Figure S2. 2D plots of the TRES for **1** and **2** in TOL and THF. The steady state emission spectra are also shown (line).

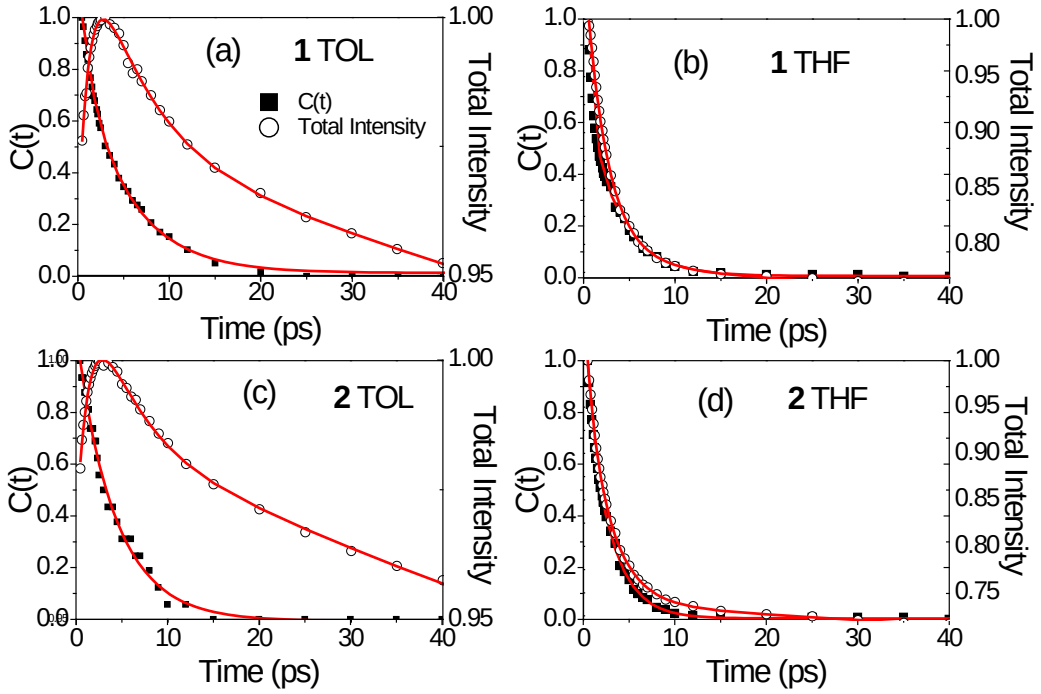

Figure S3. Solvent response function $C(t) = \frac{\nu(t)-\nu(\infty)}{\nu(0)-\nu(\infty)}$ and total area-integrated intensity of **1** and **2** in TOL and THF.

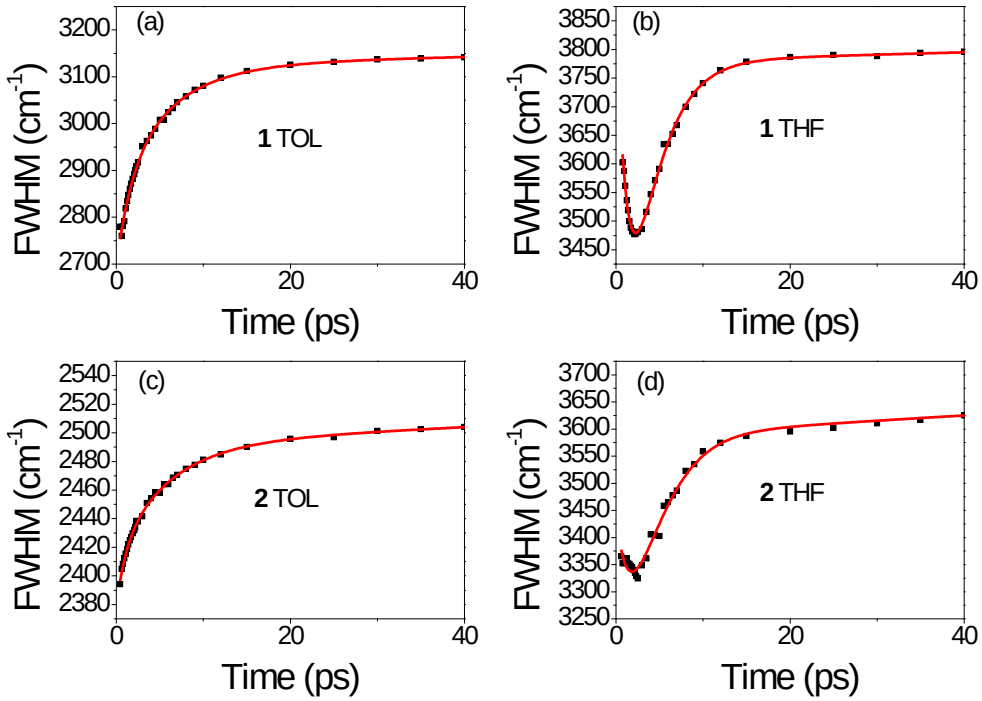

Figure S4. FWHM of the TRES as a function of time for **1** and **2** in TOL and THF.

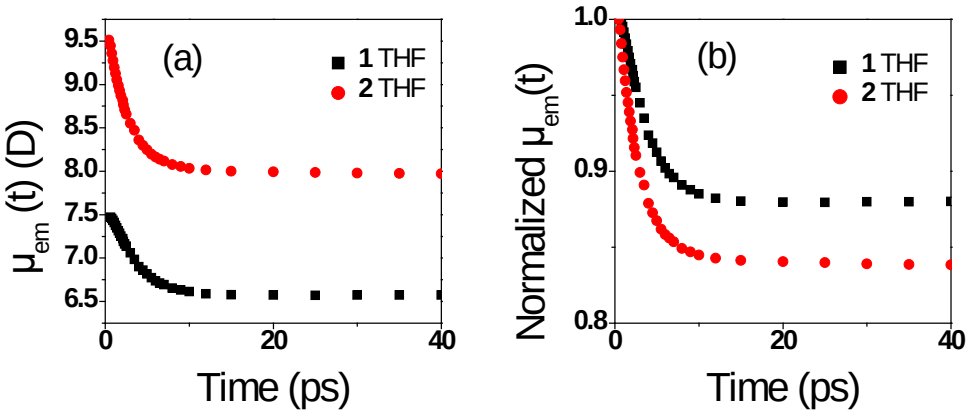

Figure S5. The non-normalized in D (a) and normalized (b) instantaneous emission dipole moments as a function of time for **1** and **2** in THF.

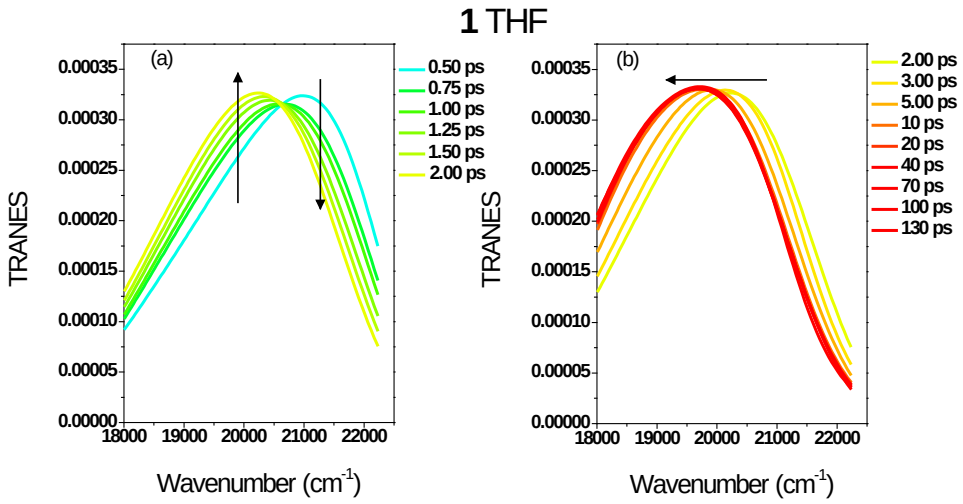

Figure S6. TRANES for **1** in THF within the (a) 0.5-2.0 ps and (b) 2.0-130 ps

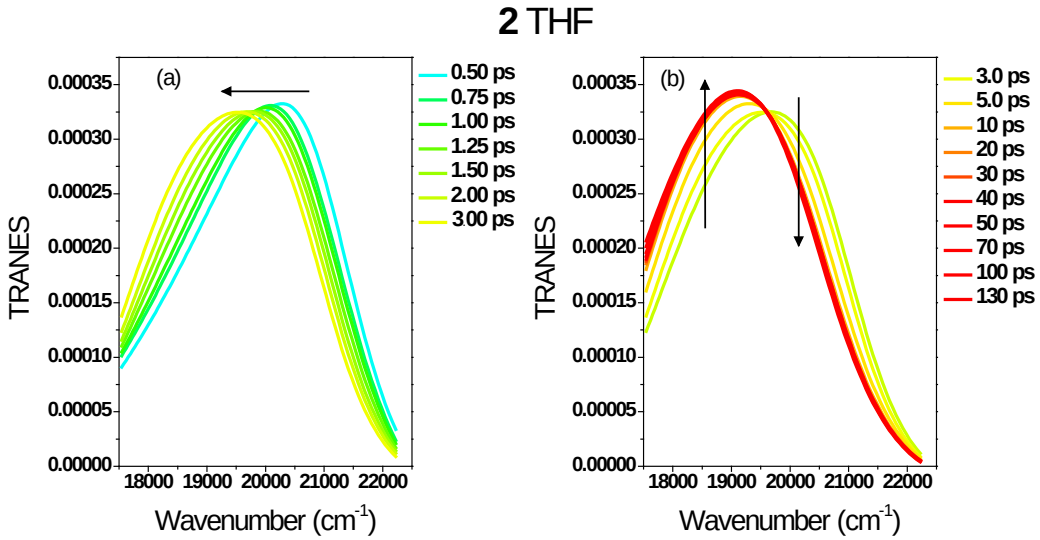

Figure S7. TRANES for **2** in THF within the (a) 0.5-3.0 ps and (b) 3.0-130 ps

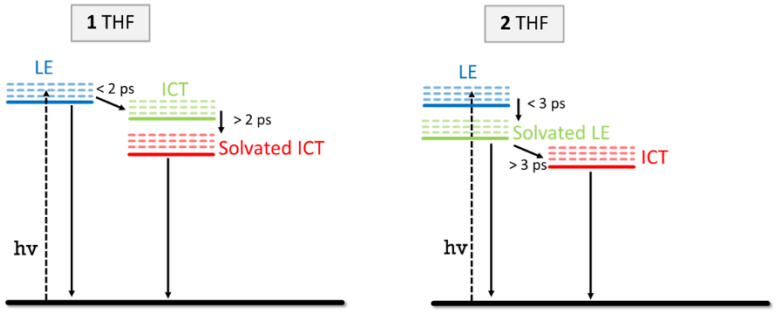

Figure S8. Schematic representation of the energy level diagram used for the explanation of the dynamics for **1** and **2** in THF.

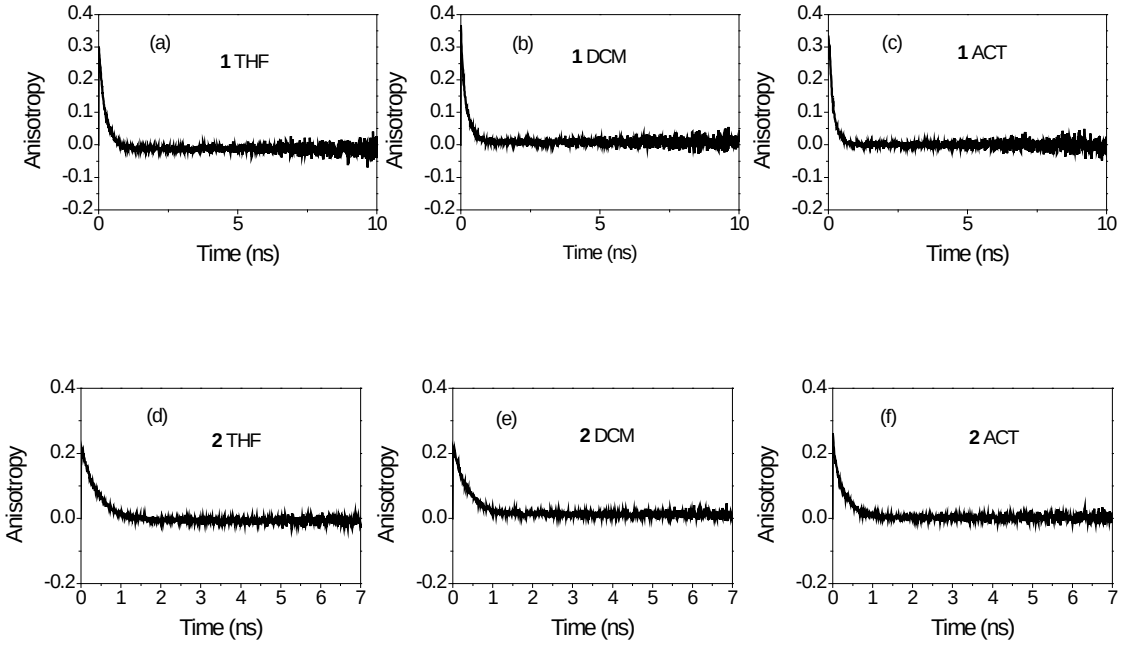

Figure S9. Anisotropy decays in the nanosecond timescale for **1** (a,b,c) and **2** (d,e,f) in selected solvents as shown in the figure.

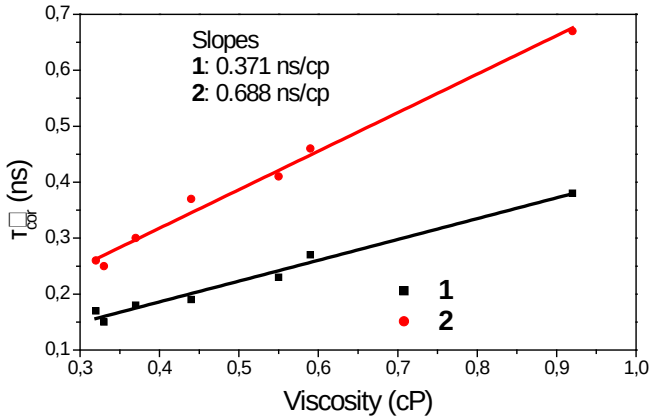

Figure S10. Correlation time versus the viscosity of the solvent for **1** and **2**.

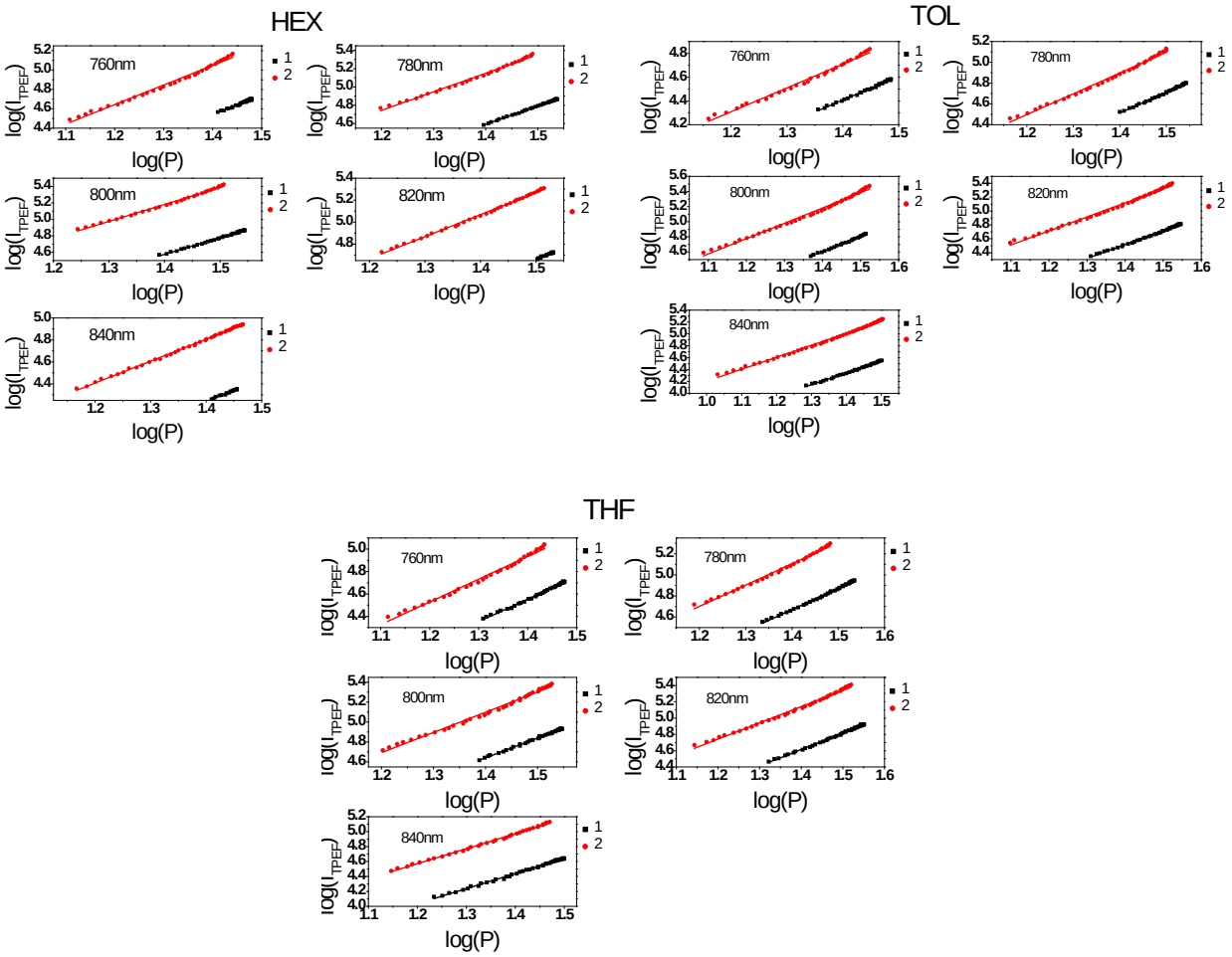

Figure S11. Plot of TPEF intensity vs. excitation laser power for compounds **1** and **2** in HEX, TOL and THF. The slopes in all cases were very close to 2.00 (R2 > 0.99) confirming the quadratic law dependence and assuring that emission is due to a two-photon induced process.

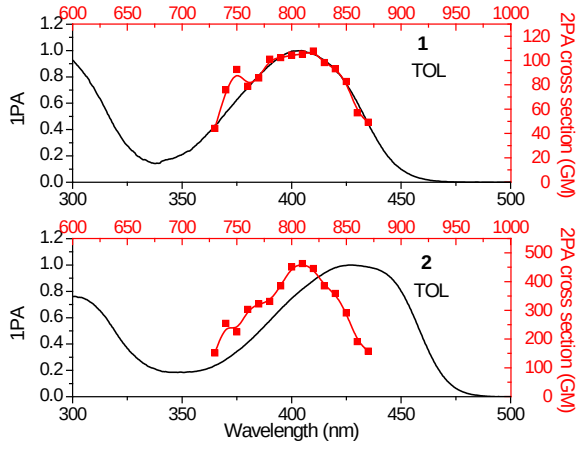

Figure S12. Comparison of 1PA and 2PA spectra for **1** and **2** in TOL.

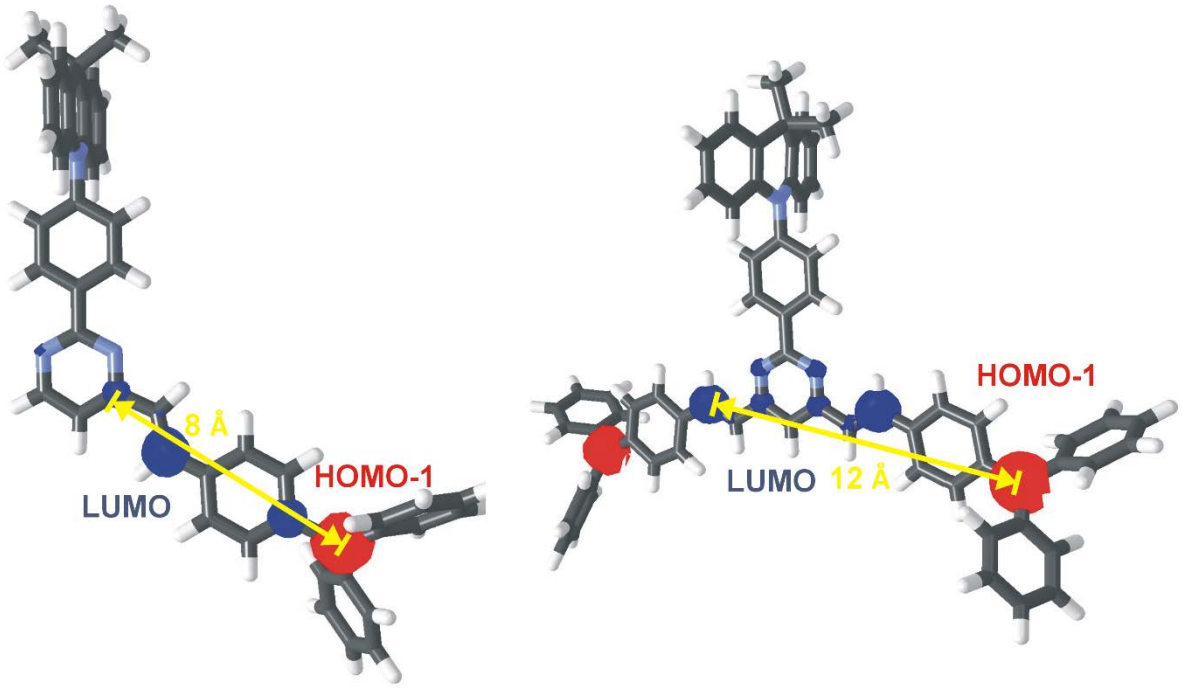

Figure S13. DFT-optimized molecular structures of **1** and **2** showing localization of the LUMO (blue) and the HOMO–1 (red) and the longest distances across both molecules where charge separation can take place, that were used to determine the Onsager cavity radius (4 and 6 Å).

1. P. K. Samanta and R. Misra, J. Appl. Phys. 2023, 133, 020901.
2. F. Bureš, RSC Adv. 2014,4, 58826.
3. H. Miranda-Salinas, Y.-T. Hung, Y.-S. Chen, D. Luo, H.-C. Kao, C.-H. Chang, K.-T. Wong and A. Monkman, J. Mater. Chem. C, 2021, 9, 8819.
4. C. Zhu, T. Wei, Y. Wei, L. Wang, M. Lu, Y. Yuan, L. Yin and L. Huang, J. Mater. Chem. A, 2021, 9, 1207.
5. Z. Zhao, C. Zeng, X. Peng, Y. Liu, H. Zhao, L. Hua, S.-J. Su, S. Yan and Z. Ren, Angew. Chem. Int Ed. 2022, 61 e202210864.
6. C. S. Abeywickrama, Chem. Commun., 2022, 58, 9855.
7. N. Yukihira, C. Uragami, K. Horiuchi, D. Kosumi, A. T. Gardiner, R. J. Cogdell and H. Hashimoto, Comm. Chem. 2022, 5,135.
8. Y.-X. Tan, X. Zhang, Y. Wang and J. Yao, Acc. Mater. Res. 2024, 5, 1377.
9. A. M. Gutiérrez-Vílchez, C. V. Ileperuma, V. Navarro-Pérez, P. A. Karr, F. Fernández-Lázaro and F. D'Souza, ChemPlusChem2024, 89, e202400348.
10. C. Qin, X. Wu, L. Tang, X. Chen, M. Li, Y. Mou, B. Su, S. Wang, C. Feng, J. Liu, X. Yuan, Y. Zhao and H. Wang, Nat Commun 2023, 14, 5238.
11. Y. Rout, C. Montanari, E. Pasciucco, R. Misra and B. Carlotti, J. Am. Chem. Soc. 2021, 143, 9933.

12. V. Maffeis, R. Brisse, V. Labet, B. Jousselme and T. Gustavsson, J. Phys. Chem. A 2018, 122, 5533.
13. D. Fan, Y. Yi, Z. Li, W. Liu, Q. Peng and Z. Shuai, J. Phys. Chem. A 2015, 119, 5233.
14. Y. Hu, C. Neumann, L. Scholtz, A. Turchanin, U. Resch-Genger and S. Eigler, Nano Research 2023, 16, 45.
15. F. Barati-Darband, M. Izadyar and F. Arkan, J. Phys. Chem. A 2019, 123, 2831.
16. Y. Li, Meng Zhou, Y. Niu, Q. Guo and A. Xia, J. Chem. Phys 2015, 143, 034309.
17. Y. Zhang, M. Jiang, G.-C. Han, K. Zhao, B. Z. Tang and K. S. Wong, J. Phys. Chem. C 2015, 119, 27630.
18. D. J. Stewart, M. J. Dalton, R. N. Swiger, J. L. Fore, M. A. Walker, T. M. Cooper, J. E. Haley and L.-S. Tan, J. Phys. Chem. A 2014, 118, 5228.
19. B. Carlotti, E. Benassi, C. G. Fortuna, V. Barone, A. Spalletti and F. Elisei, ChemPhysChem 2016, 17, 136.
20. B. Carlotti, E. Benassi, A. Spalletti, C. G. Fortuna, F. Eliseia and V. Barone, Phys. Chem. Chem. Phys., 2014, 16, 13984.
21. F. Xiao, X. Liu, K. Lin, Y. Zhou, W. Gao, Y. Lei, M. Liu, X. Huang and H. Wu, J. Phys. Chem. C 2021, 125, 16792.
22. S. Sasaki, G. P. C. Drummen and G. Konishiac, J. Mater. Chem. C 2016, 4, 2731.
23. S. Kumar, P. Singh, P. Kumar, R. Srivastava, S. Kalyan Pal and S. Ghosh, J. Phys. Chem. C 2016, 120, 12723.
24. H.-Y. Fu, X.-J. Liu, H. Zha, X.-X. Li, Y. Xu, F. Yanga and M. Xia, Phys. Chem. Chem. Phys. 2019, 21, 1399.
25. K. Hanaoka, S. Iwaki, K. Yagi, T. Myochin, T. Ikeno, H. Ohno, E. Sasaki, T. Komatsu, T. Ueno, M. Uchigashima, T. Mikuni, K. Tainaka, S. Tahara, S. Takeuchi, T. Tahara, M. Uchiyama, T. Nagano and Y. Urano, J. Am. Chem. Soc. 2022, 144, 19778.
26. R. Ghosh, Phys. Chem. Chem. Phys., 2018, 20, 6347.
27. D.-G. Chen, T.-C. Lin, Y.-A. Chen, Y.-H. Chen, T.-C. Lin, Y.-T. Chen and P.-T. Chou, J. Phys. Chem. C 2018, 122, 12215.
28. L. Martinez-Fernandez, T. Gustavsson, U. Diederichsen and R. Improta, Molecules 2020, 25, 824.
29. P. K. Singh, S. Nath, M. Kumbhakar, A. C. Bhasikuttan and H. Pal, J. Phys. Chem. A 2008, 112, 5598.
30. J. Sung, P. Kim, Y. O. Lee, J. S. Kim and D. Kim, J. Phys. Chem Lett. 2011, 2, 818.
31. B. Dereka, A. Rosspeintner, Z. Li, R. Liska and E. Vauthey, J. Am. Chem. Soc. 2016, 138, 4643.
32. B. Dereka, A. Rosspeintner, R. Stężycki, C. Ruckebusch, D. T. Gryko and E. Vauthey, J. Phys. Chem. Lett. 2017, 8, 6029.
33. F. Terenziani, A. Painelli, C. Katan, M. Charlot and M. Blanchard-Desce, J. Am. Chem. Soc. 2006, 128, 15742.
34. M. Fakis, V. Petropoulos, P. Hrobárik, J. Nociarová, P. Osuský, M. Maiuri and G. Cerullo, J. Phys. Chem. B 2022, 126, 8532.
35. J. Kong, W. Zhang, G. Li, D. Huo, Y. Guo, X. Niu, Y. Wan, B. Tang and A. Xia, J. Phys. Chem. Lett. 2020, 11, 10329.
36. R. Roy, S. Chawla, V. Sharma, A. K. Pal, Y. Silori, A. Datta, A. K. De and A. Lal Koner, Chem. Sci., 2024,15, 6363-6377.
37. A. Cesaretti, A. Spalletti, F. Elisei, P. Foggi, R. Germani, C. G. Fortuna and B. Carlotti, Phys. Chem. Chem. Phys., 2021, 23, 16739.
38. J. Wu, W. Wang, C. Gong, Q. Li, Z. Li, G. Deng, X. Zhang, K. Chen, Y. Gong and K. S. Chiangac, J. Mater. Chem. C, 2017, 5, 7472.
39. K. Senthilkumar, M. Pizzotti, K. Thirumoorthy, G. Di Carlo, S. Righetto, A. O. Biroli, M. Haukka and N. Palanisami, J. Phys. Chem. C 2016, 120, 20277.

40. J. M. Cole, R. Soc. A. 2003, 361, 2751.
41. Y. Peng, Y. Yan, P. Li, B. Li, H. Jiang, B. Guo, Q. Yuan and W. Gan, Mater. Chem. Front. 2023, 7, 502.
42. L. Sun, W. Zhu, W. Wang, F. Yang, C. Zhang, S. Wang, X. Zhang, R. Li, H. Dong and W. Hu, Angew. Chem. 2017, 56, 7831.
43. S. Sarkar, M. Santra, S. Singha, Y. W. Jun, Y. J. Reo, H. R. Kima and K. H. Ahn, J. Mater. Chem. B 2018, 6, 4446.
44. S. Pascal, Q. Bellier, S. David, P.-A. Bouit, S.-H. Chi, N. S. Makarov, B. Le Guennic, S. Chibani, G. Berginc, P. Feneyrou, D. Jacquemin, J. W. Perry, O. Maury and C. Andraud, J. Phys. Chem. C 2019, 123, 23661.
45. L. Lescos, P. Beaujean, C. Tonnelé, P. Aurel, M. Blanchard-Desce, V. Rodriguez, M. de Wergifosse, B. Champagne, L. Muccioli and F. Castet, Phys. Chem. Chem. Phys. 2021, 23, 23643.
46. F. Terenziani, C. Katan, E. Badaeva, S. Tretiak and M. Blanchard-Desce, Adv. Mater. 2008, 20, 4641.
47. M. G. Vivas, D. L. Silva, J. Malinge, M. Boujtita, R. Zaleśny, W. Bartkowiak, H. Ågren, S. Canuto, L. De Boni, E. Ishow and C. R. Mendonca, Scientific Reports 2014, 4, 4447.
48. J. Nociarová, P. Osuský, E. Rakovský, D. Georgiou, I. Polyzos, M. Fakis and P. Hrobárik, Org. Lett. 2021, 23, 3460.
49. P. Osusky, J. Nociarova, M. Smolicek, R. Gyepes, D. Georgiou, I. Polyzos, M. Fakis and P. Hrobarik, Org. Lett. 2021, 23, 5512.
50. F. Kournoutas, A. Fihey, J.-P. Malval, A. Spangenberg, M. Fecková, P. le Poul, C. Katan, F. Robin.-le Guen, F. Bureš, S. Achelle and M. Fakis, Phys. Chem. Chem. Phys. 2020, 22, 4165.
51. D. Kim, H. Moon, S. H. Baik, S. Singha, Y. W. Jun, T. Wang, K. H. Kim, B. S. Park, J. Jung, I. Mook-Jung and K. H. Ahn, J. Am. Chem. Soc. 2015, 137, 6781.
52. Y. Shen, A. J. Shuhendler, D. Ye, J.-J. Xua and H.-Y. Chen, Chem. Soc. Rev. 2016, 45, 6725.
53. Y. Morel, A. Irimia, P. Najechalski, Y. Kervella, O. Stephan, P. L. Baldeck and C. Andraud, J. Chem. Phys. 2001, 114, 5391.
54. Q. Zheng, S. K. Gupta, G. S. He, L.-S. Tan and P. N. Prasad, Adv. Func. Mater. 2008, 18, 2770.
55. G. Williams, M. Hunt, B. Boehm, A. May, M. Taverne, D. Ho, S. Giblin, D. Read, J. Rarity, R. Allenspach and S. Ladak, Nano Research 2018, 11, 845.
56. Q. Geng, D. Wang, P. Chen and S.-C. Chen, Nature Comm. 2019, 10, 2179.
57. M. Gu, Q. Zhang and S. Lamon, Nature Rev. Mater. 2016, 1, 16070.
58. J. M. Dos Santos, D. Hall, B. Basumatary, M. Bryden, D. Chen, P. Choudhary, T. Comerford, E. Crovini, A. Danos, J. De, S. Diesing, M. Fatahi, M. Griffin, A. K. Gupta, H. Hafeez, L. Hämmerling, E. Hanover, J. Haug, T. Heil, D. Karthik, S. Kumar, O. Lee, H. Li, F. Lucas, C. F. R. Mackenzie, A. Mariko, T. Matulaitis, F. Millward, Y. Olivier, Q. Qi, I. D. W. Samuel, N. Sharma, C. Si, L. Spierling, P. Sudhakar, D. Sun, E. Tankelevičiūtė, M. D. Tonet, J. Wang, T. Wang, S. Wu, Y. Xu, L. Zhang and E. Zysman-Colman, Chem. Rev. 2024, 124, 13736.
59. Z. Yang, Z. Mao, Z. Xie, Y. Zhang, S. Liu, J. Zhao, J. Xu, Z. Chi and M. P. Aldred, Chem. Soc. Rev. 2017, 46, 915.
60. Y. Tao, K. Yuan, T. Chen, P. Xu, H. Li, R. Chen, C. Zheng, L. Zhang and W. Huang, Adv. Mater. 2014, 26, 7931.
61. M. Y. Wong and E. Zysman-Colman, Adv. Mater. 2017, 29, 1605444
62. Y.Shimomura and G. Konishi, Chem. Eur. J. 2023, 29, e202301191
63. M. Mahato, T. Sultana, R. Sahoo, S. Ahamed, N. Tohora, A. Maitia and S. K. Das, Phys. Chem. Chem. Phys. 2025, 27, 1366.
64. Z. Kang, S.-C. Chen, Y. Ma, J. Wang and Q. Zheng, ACS Appl. Mater. Interfaces 2017, 9, 24771.
65. A. A. Raheem, S. Kamaraj, V. Sannasi and C. Praveen, Org. Chem. Front. 2018, 5, 777.

66. N. Altinolcek, A. Battal, C. Nur Vardalli, M. Tavasli, H. A. Yu, W. J. Peveler and P. J. Skabara, J. Mol. Struct. 2021, 1239, 130494
67. G. Tang, W. Yang and J. Zhao, J. Phys. Chem. A 2022, 126, 3653.
68. A. Karatay, H. Yılmaz, E. A. Yildiz, G. Sevinç, M. Hayvali, B. Boyacioglu, H. Unvere and A. Elmalia, Phys. Chem. Chem. Phys. 2022, 24, 25495.
69. D. Cvejn, E. Michail, K. Seintis, M. Klikar, O. Pytela, T. Mikysek, N. Almonasy, M. Ludwig, V. Giannetas, M. Fakis and F. Bureš, RSC Adv. 2016, 6, 12819.
70. Y. Gong, G.-L. Hou, X. Bi, N. Kuthirummal, A. A. Teklu, J. Koenemann, N. Harris, P. Wei, K. Devera and M. Hu, J. Phys. Chem. A 2021, 125, 1870.
71. X. Liang, B. Dong, H. Wang, Z. Zhang, S. Wang, J. Li, B. Zhao, Z. Li, Y. Xinga and K. Guo, J. Mater. Chem. C 2022, 10, 7857.
72. B. K. Kundu, G. Han and Y. Sun, J. Am. Chem. Soc. 2023, 145, 3535.
73. D. J. Stewart, R. Kannan, T. A. Grusenmeyer, J. M. Artz, S. L. Long, Z. Yu, T. M. Cooper, J. E. Haleya and L.-S. Tan, Phys. Chem. Chem. Phys. 2018, 20, 19398.
74. P. Šimon, M. Klikar, Z. Burešová, C. Vourdaki, A. Katsidas, J. Tydlitát, J. Kulhánek, J. Zelenka, M. Fakis and F. Bureš, J. Mater. Chem. C 2023, 11, 7252.
75. M. Tromayer, P. Gruber, A. Rosspeintner, A. Ajami, W. Husinsky, F. Plasser, L. González, E. Vauthey, A. Ovsianikov and R. Liska, Scientific Reports 2018, 8, 17273.
76. M. Fecková, P. le Poul, F. Bureš, F. Robin-le Guen and S. Achelle, Dyes Pigm. 2020, 182, 108659.
77. S. Achelle, M. Hodée, J. Massue, A. Fihey and C. Katan, Dyes Pigm. 2022, 200, 110157.
78. S. Achelle, J. Rodríguez-López, F. Bureš and F. Robin-le Guen, Chem. Rec. 2020, 20, 440.
79. S. Achelle, J. Rodríguez-López and F. Robin-le Guen, Org. Biomol. Chem. 2023, 21, 39.
80. M. Taniguchi and J. S. Lindsey, Photochem. Photobiol. 2018, 94, 290.
81. V. Petropoulos, I. Georgoulis, C. Vourdaki, P. Hrobárik, I. Sigmundová, J. Nociarová, M. Maiuri, G. Cerullo and M. Fakis, ChemPhysChem 2023, 24, e202300127
82. P. Hrobarik, V. Hrobarikova, I. Sigmundova, P. Zahradnik, M. Fakis, I. Polyzos and P. Persephonis J. Org. Chem. 2011, 76, 8726.
83. N. S. Makarov, M. Drobizhev and A. Rebane, Opt. Expr. 2008, 16, 4029.
84. S. de Reguardati, J. Pahapill, A. Mikhailov, Y. Stepanenko and A. Rebane, Opt. Expr. 2016, 24, 9053.
85. M. Fecková, I. K. Kalis, T. Roisnel, P. le Poul, O. Pytela, M. Klikar, F. Robin-le Guen, F. Bureš, M. Fakis and S. Achelle, Chem. Eur. J. 2021, 27, 1145.
86. C. Katan, F. Terenziani, O. Mongin, M. H. V. Werts, L.t Porrès, T. Pons, J. Mertz,, S. Tretiak,, and M. Blanchard-Desce, J. Phys. Chem. A 2005, 109, 3024.
87. L. Yan, X. Chen, Q. He, Y. Wang, X. Wang, Q. Guo, F. Bai, A. Xia, D. Aumiler, S. Vdović, and S.H. Lin, J. Phys. Chem A 2012, 116, 8693.
88. F. Terenziani, C. LeDroumaguet, C. Katan, O. Mongin and M. Blanchard-Desce, ChemPhysChem 2007, 8, 723.
89. J.E. Lewis and M. Maroncelli, Chem. Phys. Lett., 1998, 282, 197.
90. M. I. Sluch, A. Godt, U. H. F. Bunz and M. A. Berg, J. Am. Chem. Soc. 2001, 123, 6447.
91. B. Dereka, A. Rosspeintner, R. Stężycki, C. Ruckebusch, D. T. Gryko and E. Vauthey, J. Phys. Chem. Lett. 2017, 8, 6029.
92. J.R. Lacowicz Principles of Fluorescence Spectroscopy, Springer, 2006
93. M. Jia, X. Ma, L. Yan, H. Wang, Q. Guo, X. Wang, Y. Wang, X. Zhan and A. Xia, J. Phys. Chem. A 2010, 114, 7345
94. N. Periasamy and A. S. R. Koti, Proc. Indian Natn. Sci. Acad. 2003, 69, A 41.
95. P. K. Singh, M. Kumbhakar, H. Pal and S. Nath, J. Phys. Chem. B 2010, 114, 5920.

96. A. K. Mora and S. Nath, J. Phys. Chem. B 2019, 123, 8767.
97. S. R. Rather and P. Sen, J. Chem. Phys. 2013, 138, 084308.
98. S. Santra, A. K. Mora and S. Nath, J. Photochem. Photobiol. A Chem. 2023, 437, 114474.
99. M. L. Horng, J.A. Gardecki, A. Papazyan and M. Maroncelli, J. Phys. Chem. 1995, 99, 17311.
100. L. Reynolds, J. A. Gardecki, S. J. V. Frankland, M. L. Horng and M. Maroncelli, J. Phys. Chem. 1996, 100, 10337.
101. J. S. Beckwith, A. Rosspeintner, G. Licari, M. Lunzer, B. Holzer, J. Fröhlich and E. Vauthey, J. Phys. Chem. Lett. 2017, 8, 5878.
102. X. Niu, Z. Kuang, M. Planells, Y. Guo, N. Robertson and A. Xia, Phys. Chem. Chem. Phys. 2020, 22, 15743.
103. N. S. Makarov, S. Mukhopadhyay, K. Yesudas, J.-L. Brédas, J. W. Perry, A. Pron, M. Kivala and K. Müllen, J. Phys. Chem. A 2012, 116, 3781.
104. C. Sissa, V. Parthasarathy, D. Drouin-Kucma, M. H. V. Werts, M. Blanchard-Desce and F. Terenziani, Phys. Chem. Chem. Phys. 2010, 12, 11715.
105. L. Li, Y.-P. Tian, J.-X. Yang, P.-P. Sun, J.-Y. Wu, H.-P. Zhou, S.-Y. Zhang, B.-K. Jin, X.-J. Xing, C.-K. Wang , M. Li, G.-H. Cheng, H.-H. Tang, W.-H. Huang, X.-T. Tao and M.-H. Jiang, Chem. Asian J. 2009, 4, 668.
106. B. Liu, X.-L. Hu, J. Liu, Y.-D. Zhao and Z.-L. Huang, Tetrahedron Lett. 2007, 48, 5958.
107. Q. Zhang, L. Luo, H. Xu, Z. Hu, C. Brommesson, J. Wu, Z. Sun, Y. Tian and K. Uvdal, New J. Chem. 2016, 40, 3456.
108. A. Rebane, M. Drobizhev, N. S. Makarov, G. Wicks, P. Wnuk, Y. Stepanenko, J. E. Haley, D. M. Krein, J. L. Fore, A. R. Burke, J. E. Slagle, D. G. McLean and T. M. Cooper, J. Phys. Chem. A 2014, 118, 3749.
109. A. Rebane, M. Drobizhev, N. S. Makarov, E. Beuerman, J. E. Haley, D. M. Krein, A. R. Burke, J. L. Flikkema and T. M. Cooper, J. Phys. Chem. A 2011, 115, 4255.